Chapter 13 Discussion

13.1 Introduction

The discussion of the results given in the previous chapter is divided into four parts:

- the first part, which comprises section 13.2 and 13.3, deals with the equilibrium solubility trends of AlN in low and high sulphur low carbon Al-killed hot rolled strip steels during reheating;
- the second part, which consists of section 13.4, deals with the study of the concurrent static recrystallisation and precipitation of AlN during isothermal annealing of the cold worked steels HS140-104, HS90-12, LS70-38 and LS2-65 in the as-quenched condition;
- the third part, which is in section 13.5, presents the recrystallisation behaviour in laboratory simulated coiled steels HS140-104, LS70-38 and LS2-65 in which the sulphur content and the simulated coiling temperatures were varied; and
- the last part, which is in section 13.6, deals with the nucleation of AlN on MnS particles during hot rolling and coiling and its impact on the static recrystallisation after cold working in these steels.

13.2 Effect of soaking time on the dissolution of the AlN

In figure 12.1, the relative TEP values $\triangle S$ are plotted against the isothermal soaking times at 1150 °C for high and low sulphur content steels HS140-104 and LS2-65 respectively. Assuming that

the contribution from lattice defects and other substitutional alloying elements was negligible and/or the same for all of these specimens, the measured relative TEP value ΔS after quenching from the solution treatment temperature represented the carbon and nitrogen in solid solution. At this solution treatment temperature of 1150 °C, the carbon was already completely in solid solution and, therefore, any variations in measured TEP values could be attributed to the partial or complete dissolution of the AlN particles.

As may be seen in figure 12.1, there was no significant change in the relative TEP values after about 5 minutes and up to 20 minutes soaking times and this meant that no further significant dissolution of AlN took place after soaking the steels for more than 5 minutes. The soaking time of about 5 minutes or more was, therefore, adequate to achieve equilibrium conditions during AlN solution heat treatment of these two steels, which were at the extreme limits of the range of sulphur contents used here. This already suggests that differences in the sulphur levels in these steels do not affect the kinetics of equilibrium dissolution of the AlN after soaking for 5 minutes or more at a solution treatment temperature of 1150 °C. The differences in the relative TEP values were, therefore, only due to the differences in nitrogen content whereby the steel with the higher nitrogen content registered higher TEP values. Similar observations were made by Mayrhofer et al[47] that, during AlN solution treatment even in the presence of coarse AlN, equilibrium was achieved in less than 10 minutes at temperatures above 1000 °C. It may, therefore, be concluded that

Chapter 13 Discussion

AlN dissolves relatively quickly in low carbon Al-killed steels during a solution or reheating treatment.

13.3 Equilibrium solubility trends during reheating of AlN in low carbon Al-killed strip steels with low and high sulphur contents

As may be seen in both figures 12.2 and 12.3, there is some scatter in the TEP results and this may possibly be attributed to quenched-in defects, presence of coherent or semi-coherent particles and interaction of nitrogen and carbon with other alloying elements in these commercial low carbon strip steels. Interstitials that segregate to dislocations and other lattice defects may not contribute measurably to the TEP effect any more while the strain field around coherent particles and lattice defects such as dislocations, on the other hand, may do so[(147)]. As a result there will be some variation in TEP measurements from such metallurgical effects and, of course, also from purely extraneous experimental effects in measurement. However, the R-squared value (R^2 = 0.8) from the regression analysis in figure 12.3, shows that the effects of the scatter are still reasonable.

In order to correlate the nitrogen content in solid solution to the measured relative TEP or $\triangle S$ values, some assumptions had to be made:

Chapter 13 Discussion

(a) All the nitrogen had precipitated into coarse and incoherent AlN during the prior annealing process at 800 °C for 6 hours and that the nitrogen in solid solution that was in equilibrium with the AlN at that temperature, was negligible. This assumption was tested with an existing AlN equilibrium solubility equation in ferrite (equation 13.3 below) and it predicts that at 800 °C, only about 3 ppm of the nitrogen would be in solid solution[38].

(b) All the nitrogen was in solid solution at the points where the TEP measurements leveled off after the specimens had been solution treated at higher temperatures, as was shown in figure 12.2.

(c) TEP contributions from other dissolving substitutional alloying elements were negligible and/or constant.

(d) TEP contributions from quenched-in lattice defects were negligible and/or constant.

(e) As TEP measurements were done at room temperature and the fact that all the steels that were studied were low carbon steels with a maximum of 0.058%C and 104 ppm N, the specimens were fully ferritic and there were no TEP contributions from matrix phase variations.

The amount of nitrogen in solid solution could then be deduced from the Gorter-Nordheim law[135] using equation 10.2 ($\triangle S_N$ =

$S_{800} - S_i = K_{AlN}[N]$). The amount of aluminium required to combine with the nitrogen was calculated from the stoichiometric composition of AlN, which was less than the analysed acid soluble aluminium content for all the steels that were studied, see chemical compositions in table 10.1.

The equation from the regression analysis of the plot of the logarithm of the solubility product of the AlN, i.e. Log[%Al][%N], versus the inverse of the absolute solution treatment temperature in figure 12.3, is the equilibrium solubility equation for the AlN in austenite in these steels as determined by the TEP technique and was found to be:

$$\text{Log}[\%\text{Al}][\%\text{N}] = 2.6 - \frac{9710}{\text{T}} \qquad (13.1)$$

where the aluminium and the nitrogen contents are in weight percentage and T is the absolute solution temperature in Kelvin.

From figure 12.3, the most important observation is that the sulphur content does not appear to have any measurable effect on the equilibrium solubility of the AlN in these steels, at least within the experimental scatter found, i.e. the AlN equilibrium solubility of both the low and high sulphur steels that were studied could be modelled by the same equation 13.1. This is in agreement with the observations made by many workers in these steels using other techniques than TEP[41-52].

Chapter 13 Discussion

The results in figure 12.3 were checked by Thermo-Calc and the results predicted that sulphur should not influence the equilibrium solubility of AlN in low carbon Al-killed steels, see figure 12.4. This was not surprising as Thermo-Calc employs similar thermodynamic models (given in the appendix) to compute the solubility limits of the AlN.

The AlN equilibrium solubility model from this work is compared with models from others workers in figure 13.1 below. The results from this study give slightly higher solubility limits when compared with the results obtained through the Beeghly technique and could be due to a number of reasons arising from the different techniques employed. While the TEP technique is based on the assumptions made above, the Beeghly technique also has its own shortfalls, mainly the lack of sensitivity to particles of less than 10 nm in diameter and its failure to isolate the AlN from other nitrides[42]. Consequently, lower solubility temperatures are reported by the Beeghly technique compared to other techniques.

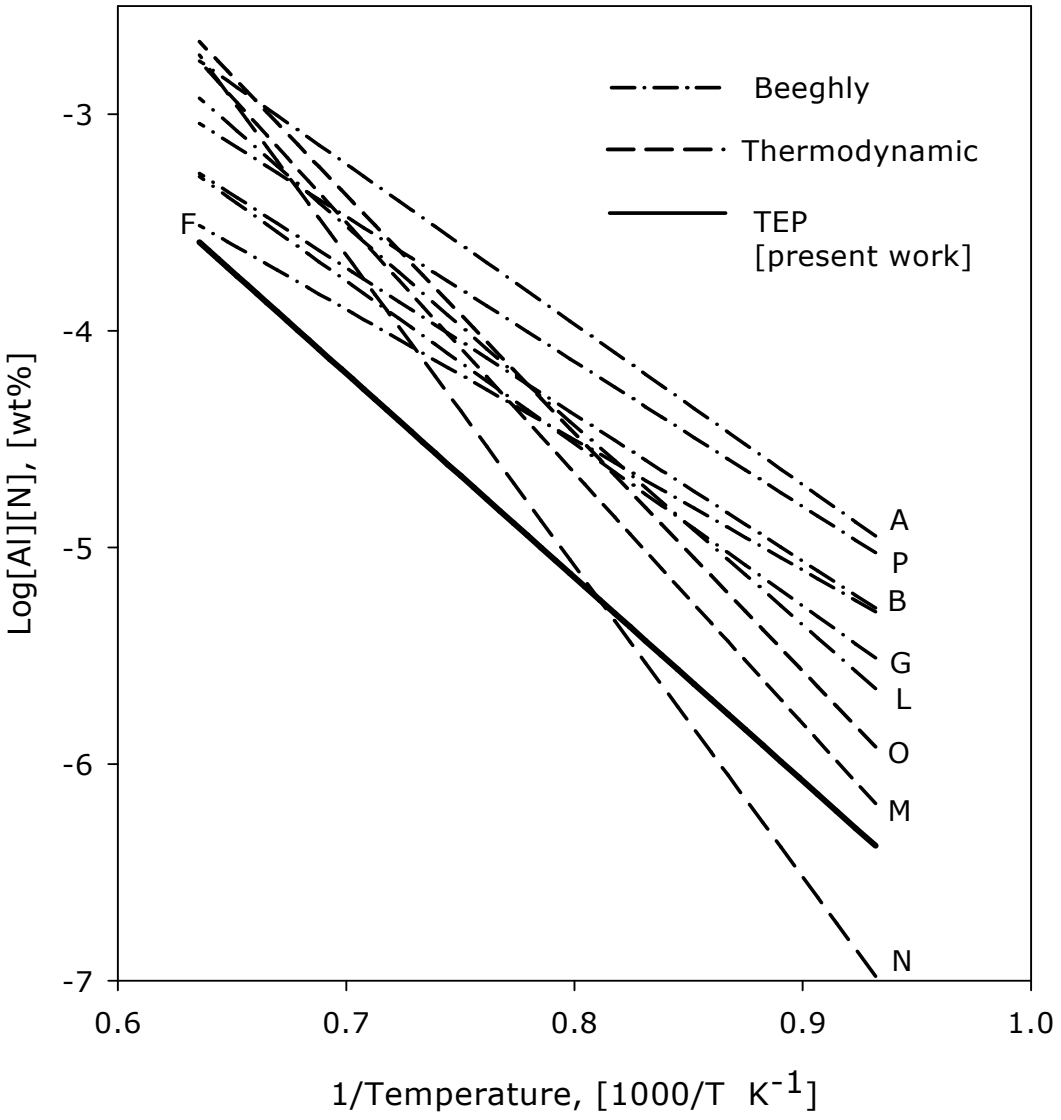

Figure 13.1: Comparison of the TEP equilibrium solubility model from this work with the models from other authors; details for the other curves are given in the appendix.

Curves M, N and O in figure 13.1 were calculated from thermodynamic data and are based on the Fe-Al-N system[49-51].

Hence, any possible interactions of the AlN with other alloying elements, as may be the case in commercial strip steels, are not taken into account by this approach. This may account for the difference between the solubility model from this work and those derived from the thermodynamic data.

Despite the differences in the predicted AlN solubility limits, all models including the one from this work, indicate that the sulphur content in these low carbon Al-killed strip steels does not influence the equilibrium solubility of AlN.

It may be worthwhile to also compare the TEP coefficient K_{AlN} for AlN from this work with those from other work. Using equation 10.2 and with the assumptions regarding TEP measurements made above, the solubility coefficient K_{AlN} is given by:

$$K_{AlN} = \frac{\left(S_{800} - S_f\right)}{[N]} = \frac{\Delta S}{[N]}$$

where S_{800} is the absolute TEP measurement for the specimen that was solution treated at 800 ºC for 6 hours, S_f is the absolute TEP value at the solution temperature where the absolute TEP values level off and $[N]$ is the nitrogen content in solid solution, in this case the one that was obtained from the LECO analyses.

Values of the TEP coefficient K_{AlN} for AlN obtained in this work are compared with values from the literature in table 13.1.

Chapter 13 Discussion

Table 13.1: TEP coefficients K_{AlN} for AlN obtained from the five steels that were studied and compared to published values.

Steel	N [ppm]	ΔS [μV/K]	K_{AlN} [$x10^{-9}$ V/K.ppm]	Literature [$x10^{-9}$ V/K.ppm]
HS130-50	50	0.43	8.6	6.7 to 10 (Biron et al[148])
HS90-34	34	0.21	6.4	
HS140-104	104	0.79	7.6	
LS10-83	83	0.63	7.5	
LS2-65	65	0.46	7.1	

As may be seen from table 13.1, the TEP coefficients for AlN obtained in this work are in good agreement with those obtained by Biron et al[148] on low carbon (0.02 to 0.066%C) and 17 to 102 ppm nitrogen Al-killed steels.

The TEP results were checked by TEM on carbon extraction replicas and the results are given in figures 12.5 to 12.8. After isothermal annealing at 800 °C for 6 hours, the AlN had precipitated into coarse cuboids and fine round particles as shown in figure 12.5. When these specimens were solution treated at higher temperatures in order to dissolve the AlN, in the medium nitrogen steel LS2-65 the AlN disappeared at 1200 °C and this was somewhat higher by nearly 50 °C than the dissolution temperature determined by the TEP technique, which was about 1150 °C. The difference might be due to the scatter in the TEP results, see figure 12.3. As for steel HS140-104, there was good

agreement between the dissolution temperature determined by TEM on carbon extraction replicas and the TEP technique as no more AlN could be observed after a soaking temperature of 1250 °C, see figure 12.8.

13.4 Concurrent static recrystallisation and precipitation of AlN during isothermal annealing of a low carbon Al-killed cold worked steel HS140-104 in an as-quenched condition

Steel HS140-104 was solution treated at 1300 °C for 12 minutes to dissolve both the AlN and MnS and quenched into water (see figure 10.1), cold worked 70 percent, and isothermally annealed at 610 °C to induce static recrystallisation. Figure 12.9 shows the progression of the recrystallisation process and it is evident from the micrographs that between 5 and 18 minutes, there was a complete recrystallisation arrest i.e. there was no significant increase in the recrystallised volume fraction with an extension of the isothermal annealing time. This observation was supported by the quantitative results given in figure 12.12 in which the recrystallised volume fraction was plotted against the isothermal annealing time, see the cross hatched area. However, no recrystallisation arrest was observed in this steel at temperatures of 580 °C and below or above 700 °C, see figures 12.10 and 12.12.

Chapter 13 Discussion

A recrystallisation arrest in Al-killed low carbon steels within the intermediate temperature range of 550 to 650 °C, has also been observed by other workers and was attributed to the clustering or nucleation of AlN[8,9,119]. It was reported that at an isothermal annealing temperature of 550 °C and below, AlN precipitation precedes recrystallisation while at temperatures higher than 650 °C the latter precedes the former. However, in this study, it was observed that even at 580 °C, AlN still preceded recrystallisation and, therefore, this suggests that the lower temperature limit may also depend on the chemical composition and the supersaturation of the nitrogen and aluminium of the steel. Both of these will reflect in the ratio V_v/r which dictates effective Zener pinning above a certain critical value.

It was also established that in cold worked low carbon Al-killed steels, AlN nucleates predominantly on dislocation sub-boundaries whereas grain boundaries are preferred nucleation sites in recrystallised material[11,122,149], probably due to a lack of dislocations and subgrain boundaries. As a result, the recrystallisation process is inhibited through particle pinning of the dislocation sub-boundaries as well as the recrystallisation interfaces in what is commonly called the "Zener drag" or "Zener pinning" effect.

As may be seen from figure 12.13, there was no significant difference between the as-quenched material and the one that was annealed at 450 °C for 30 minutes to precipitate the Fe_3C prior to cold working. The presence of carbon in or out of solution,

therefore, does not appear to affect the kinetics of the recrystallisation process. It, therefore, appears that the precipitation of AlN and not Fe_3C may be responsible for the recrystallisation arrest, with the start of the arrest time, representing the start time for AlN nucleation that becomes effective in Zener drag. This start time was estimated from the crossing point of an extrapolation of the horizontal arrest plateau and the slope of the rising curve in Figure 12.12 just before the arrest started.

The arrest finish time should also represent a stage where the particle size of the AlN becomes ineffective for Zener drag on moving recrystallisation interfaces and this time is assumed to be associated with the "end of nucleation", i.e. the time where there are no new very small precipitates that are forming and that can still exercise Zener drag. This time was also estimated through the extrapolation of the two lines as indicated above for the start time.

While it is impossible to observe directly by electron microscopy the very early stages of the precipitation of AlN and its effect on the recrystallisation process in cold worked material, it was observed in this work that the apparent activation energy of the process that led to the recrystallisation arrest was 230 kJ mol^{-1}, and this was somewhat close to that for the diffusion of aluminium in the matrix of α-ferrite which is quoted as 196.5 kJ mol^{-1} [149], see figure 12.14. The observed value of 230 kJ mol^{-1} differs slightly from that obtained by Ogawa et al[150] in an assessment of

the activation energy for the precipitation of AlN in both annealed and cold worked iron, which was reported as 243 kJ mol^{-1}. Biron et al[148] used the TEP technique to assess this same activation energy in Al-killed low carbon-manganese steels and also found a value of 243 kJ mol^{-1}. Using the same TEP technique, however, Brahmi et al[144] observed two temperature regimes for the nucleation of AlN in an Fe-Al-N alloy with different activation energies; the first was 250 kJ mol^{-1} for the temperature range of 500 to 575 °C and the second was 210 kJ mol^{-1} for the range of 600 to 700 °C. Due to the high diffusivity of nitrogen in ferrite, it is generally assumed that no rate controlling nitrogen concentration gradient will occur during nucleation and growth of AlN and, therefore, the diffusion of aluminium atoms is likely to be rate controlling in the precipitation of AlN[11,55].

13.4.1 Modelling the activation energy for the nucleation of AlN in ferrite, ΔG^*_{AlN} and the critical radius r*

The classical model for the rate of homogeneous nucleation of AlN is given by equation 3.16 and is as follows[28,29]:

$$\dot{N}_{AlN} = N_0 Z \beta Exp\left[-\frac{\left(Q_{D(Al)} + \Delta G^*_{AlN}\right)}{RT}\right] \qquad (13.2)$$

where $Q_{D(Al)}$ is the activation energy for the diffusion of aluminium in ferrite, ΔG^*_{AlN} is the activation energy for the

nucleation of AlN in ferrite and the rest is as defined in equation 3.16.

The activation energy for the isothermal and homogeneous nucleation of AlN in ferrite is modelled using data from literature, which are given in table 13.2.

Table 13.2: Parameters that have been used to calculate the activation energy for the isothermal and homogeneous nucleation of AlN in ferrite ΔG^*_{AlN}.

Parameter	Values	Reference
Interface energy, (J m^{-2})	0.2	151
Enthalpy of formation of AlN in ferrite ΔH, (kJ mol^{-1})	138	49
Bulk Modulus K for AlN (GPa)	210	152
Shear Modulus G_m for AlN (GPa) $G_m = \frac{\left(\frac{3}{2}\right)K(1-2\nu)}{1+\nu}$	151	
Poisson's ratio ν of AlN	0.21	152
Lattice parameter of fcc AlN a_{AlN} (nm)	0.4071	38
Lattice parameter of bcc iron a_{Fe} (nm)	0.286	153
Density of AlN (kg m^{-3})	3200	35
Molar volume V_m for AlN (m^{-3} mol^{-1})	1.28 x 10^{-5}	

Chapter 13 Discussion

Previous studies have shown that AlN nucleates with a coherent cubic (NaCl-type) crystal structure and with a Bain crystallographic orientation relationship with respect to the bcc iron matrix[37-39]. Using equation 3.12, the resulting misfit strain is calculated as:

$$\text{Misfit, } \quad \delta = \frac{\left(0.407-\left(\sqrt{2}\ \text{x}\ 0.286\right)\right)}{0.286} = 8.86 \text{ x } 10^{-3}$$

Since this study did not cover the equilibrium solubility of AlN in ferrite but only in austenite, the enthalpy of formation of AlN in α-iron has been derived from the AlN equilibrium solubility model given in reference 38 and using equation 4.3 ($\triangle H = 1.15RA$). The equilibrium solubility equation for the AlN in α-ferrite is given as follows:

$$\text{Log}[\%\text{Al}][\%\text{N}] = 6.061-\frac{14442}{\text{T}} \qquad (13.3)$$

where both the aluminium and the nitrogen content are in weight percent and the absolute temperature T is in Kelvin.

At equilibrium, the driving force for the isothermal nucleation of AlN in ferrite, in this case during isothermal annealing at 610 °C, has been calculated from equation 3.7 as:

$$\Delta G_v = \Delta H\left(\frac{\Delta T}{T_e}\right) = 138000\left(\frac{668}{1550}\right) = 59.5 \text{ kJ mol}^{-1}$$

where the equilibrium solubility limit temperature T_e (in K) has been predicted from the solubility model developed from this work, equation 13.1, to be about 1280°C.

For homogeneous nucleation and negligible strain energy around the nucleus, the activation energy ΔG^* for isothermal nucleation of a particle of critical radius r^* is given by equation 3.6 as:

$$\Delta G^*_{AlN} = \frac{16\pi\gamma_s^3 V_m^2}{3(\Delta G_v)^2} = 6.2 \times 10^{-21} \text{ J}$$

where a value of the surface energy γ_s of 0.2 J m^{-2} for a coherent interface of the AlN in ferrite has been used[151].

The critical radius r^* for homogeneous nucleation without strain energy around the embryo is given by equation 3.5 i.e.:

$$r^*_{AlN} = \frac{-2\gamma_s V_m}{\Delta G_v} = 8.6 \times 10^{-11} \text{ m}$$

This modelled value of the critical radius r^* is very small and appears to be less than the size of an aluminium atom (~0.14 nm). This might be as a result of the overestimation of the driving force ΔG_v or underestimation of the surface energy γ_s or a combination of both. However, AlN particles of about 15 nm in size were observed in these steels and, therefore, it is believed that the critical radius r^* should actually be somewhere between about 3 and 10 nm, where the latter is the estimated lower limit

of effective observation in thin foil TEM. The fact that the value of the critical radius r^* diminishes to practically zero ($r^* \rightarrow 0$) may signify that AlN nucleates with ease in ferrite at temperatures above 600 °C as already observed by other workers[65].

By dividing and multiplying the activation energy ΔG^*_{AlN} per critical radius (of an assumed value of $r^* = 3$ nm) by the volume of the critical radius ($V^* = 1.13 \times 10^{-25}$ m^3) and the molar volume of AlN ($V_m = 1.28 \times 10^{-5}$ m^3 mol^{-1}) respectively the modelled activation energy ΔG^*_{AlN} for homogeneous nucleation of AlN in ferrite during isothermal annealing at 610 °C becomes 0.7 J mol^{-1}. This seems very low compared with the value observed in this work of about 30 kJ mol^{-1} i.e. ($Q_{D(Al)} + \Delta G^*_{AlN}$) = 230 kJ mol^{-1} where $Q_{D(Al)}$ has been found elsewhere[149] to be 196.5 kJ mol^{-1}. The discrepancy might be a result of overestimation in the assumed values of the critical radius r^* or/and the driving force ΔG_v. Therefore, the value of 30 kJ mol^{-1} may be a realistic estimation of the activation energy for the nucleation of the AlN in ferrite.

The strain energy ΔG_ε resulting from a coherent interfacial misfit of the AlN/ferrite interface, is very small if compared to the chemical driving force ΔG_v and was neglected in the calculation for r^* and ΔG^* above. Its size may be estimated through equation 3.13 i.e.:

Chapter 13 Discussion

$$\Delta G_{\varepsilon-coh} = \frac{6G_m V^* \delta^2}{\left[1+\frac{4G_m}{3K}\right]} = 4.1 \times 10^{-18} \text{ J}$$

$$= 460 \text{ J mol}^{-1}$$

where V* is the volume of the critical radius r* of the AlN embryo.

The rather relatively small value of the activation energy ΔG^*_{AlN} for the homogeneous nucleation of AlN in ferrite of 30 kJ mol^{-1} is not surprising because previous workers[44] have found that in α-ferrite the isothermal nucleation of AlN is controlled by the diffusion of aluminium (which means that the activation energy for nucleation, must be very low in comparison) while at higher temperatures and in austenite, it is limited by the nucleation barrier i.e. by a high activation energy ΔG^*_{AlN} [44,47,153,154]. The modelled low strain energy of 460 J mol^{-1} is the result of a low misfit (δ = 8.86 x 10^{-3}) between the coherent cubic structure of AlN and the α-ferrite matrix. Furthermore, the activation energy for nucleation of AlN in ferrite may even reduce further than the above estimated 30 kJ mol^{-1} if the reported heterogeneous nucleation on subgrain boundaries and dislocations of AlN is considered.

The results from this work, therefore, confirm that $Q_{D(Al)} >> \Delta G^*_{AlN}$ i.e. $(Q_{D(Al)} + \Delta G^*_{AlN}) \approx Q_{D(Al)}$, and $\Delta G^*_{AlN} \rightarrow 0$. This leads to the conclusion that the activation energy for the nucleation of AlN is very small and may be ignored without affecting its

predicted nucleation rate. The nucleation rate of AlN in ferrite should, therefore, be very high and it may be assumed that in an as-quenched microstructure during annealing at 610°C in these steels, that the nucleation of the AlN is over relatively quickly with effective recrystallisation arrest through Zener pinning setting in soon thereafter. This means that the recrystallisation arrest, which is associated with the diffusion of aluminium, can indeed be used to indirectly observe the start of precipitation of AlN in cold worked low carbon Al-killed strip steels as:

$$\frac{\left(P_{start} - Z_{start}\right)}{\left(P_{start} - P_{finish}\right)} \rightarrow 0 \qquad (13.4)$$

and

$$\frac{\left(P_{finish} - Z_{finish}\right)}{\left(P_{start} - P_{finish}\right)} \rightarrow 0 \qquad (13.5)$$

where P_{start} is the AlN precipitation start time, Z_{start} is the recrystallisation arrest start time, P_{finish} is the AlN precipitation finish time and Z_{finish} is the recrystallisation arrest finish time.

Figure 12.15 may, therefore, represent a reasonable estimate of the TTT-diagram for the precipitation of AlN in ferrite in cold worked material, as measured indirectly from this arrest-effect.

Since this method of estimating the TTT diagram for AlN is based on the recrystallisation arrest effect, the end of the arrest, Z_{finish} may not necessarily mean the end of growth by supersaturation i.e. the AlN precipitation finish time P_{finish} (which is generally

included in the classical process of nucleation) but it does represent the end of "particle effectiveness" which is due to coarsening and may, therefore, reasonably represent the end of the precipitation process.

13.4.2 Recrystallisation in an as-quenched condition of the steels with various nitrogen and sulphur contents

Steels HS140-104 , LS70-38, LS2-65 and HS90-12 were solution treated at 1300 °C for 12 minutes to dissolve both the AlN and MnS and quenched into water (see figure 10.1), cold worked 70 percent, and isothermally annealed at 610 °C to induce static recrystallisation.

At the beginning of the isothermal annealing process directly after quenching from solution treatment, both the aluminium and the nitrogen were in solid solution and the volume fraction of the precipitated AlN during the isothermal annealing process can be predicted from the equilibrium solubility of AlN in ferrite which is given in equation 13.3 ($\log[\%Al][\%N] = 6.061-14442/T$) and it is found to be less than 1 ppm of nitrogen in solid solution at a temperature of 610 °C.

Sennour et al[38] also observed that the AlN had a stoichiometric composition and with this information the volume fraction of precipitated AlN can be estimated. Assuming that the volume fraction of the other alloying elements in solution in these steels

are negligible compared with that of iron, the volume fraction V_v of the AlN is given by:

$$V_v = \frac{(m/\rho)_{AlN}}{(m/\rho)_{Fe} + (m/\rho)_{AlN}} \qquad (13.6)$$

where m and ρ are the weight percentages and the densities of the respective elements. The densities of iron and AlN are taken as 7.8 and 3.2 g cm^{-3} respectively.

The estimated volume fractions V_v of the precipitated AlN during isothermal annealing at 610 °C in the four steels that were studied in this series, are given in table 13.3 below.

In this study, the recrystallisation arrest was observed in the steels with nitrogen content of 65 ppm and above while none was observed for the steels with nitrogen content of 38 ppm and less. Assuming that nucleation by site saturation condition was met and that during the early stages of nucleation and growth of the AlN, the mean particle size for all four steels in table 13.3, did not vary much from steel to steel, then the difference in the Zener pinning effect, which is governed by the ratio (V_v/r), would be proportional to the volume fraction V_v of the particles which, in turn, is dependent on the chemical composition of the steel. Therefore, it is not surprising that no recrystallisation arrest was observed in the lower nitrogen steels LS70-38 and HS90-12 with AlN volume fractions of only 2.67×10^{-4} and 8.4×10^{-5} respectively, see figures 12.11 and 12.16.

Chapter 13 Discussion

Table 13.3: Estimated volume fraction V_v of the precipitated AlN during isothermal annealing at 610 °C in 70 percent cold worked steels HS140-104, LS70-38, LS2-65 and HS90-12.

Steel	N (%wt)	Al (%wt) (acid soluble)	Estimated V_v ($x10^{-4}$)
HS140-104	0.0104	0.047	7.29
LS2-65	0.0065	0.037	4.56
LS70-38	0.0038	0.02	2.66
HS90-12	0.0012	0.039	0.84

It also needs to be recognised that within the isothermal annealing temperature range of 550 to 700 °C, there must have been other alloying elements which were diffusing out of solid solution as well, among them manganese, copper and sulphur, see figure 5.1. However, it has been observed from this work that in low nitrogen but high sulphur material, for instance in steel HS90-12 with a very low volume fraction of AlN (8.4×10^{-5}), there was no recrystallisation arrest, see figure 12.16. This suggests that it was the AlN precipitation alone that was responsible for the recrystallisation arrest that was observed in the medium to high nitrogen steels, HS140-104 and LS2-65 where the volume fraction V_v of AlN was sufficiently high ($V_v \geq 4.555 \times 10^{-4}$) to provide an effective arrest.

The results in figure 12.16 also show that the steels with a lower sulphur content in solid solution, i.e. steels LS2-65 and LS70-38, despite having higher a nitrogen content than steel HS90-12,

recrystallised at earlier times compared to the steels with higher sulphur content, such as steels HS140-104 and HS90-12. The advantage of a lower nitrogen content with regards to a faster recrystallisation process in steel HS90-12, was completely overshadowed by the higher sulphur content in solid solution. This observation is in agreement with the results of Jolley et al[120] that the sulphur content in solid solution retards the start of the recrystallisation process by segregating to dislocation sub-boundaries and recrystallisation fronts in low carbon-manganese steels, see the earlier figure 7.2. However, as was observed in this work, the sulphur does not necessarily cause a complete recrystallisation arrest as in the case with the nucleation ("clustering") of AlN. It appears that the higher sulphur content affected the incubation period of the recrystallisation process through boundary drag rather than affecting the kinetics as the Avrami exponents for both the low and high sulphur content steels were the same, i.e. $n \approx 1$ see figure 12.17, but the values for the MAJK constant k differed significantly; 0.18 for the low sulphur content steel LS2-65 and 0.042 for the higher content one, steel HS140-104.

13.4.3 Modelling the Zener drag force P_z in steel HS140-104 in the as-quenched and cold worked condition during isothermal annealing at 610 °C

The loss in Zener pinning effect as the annealing time is extended can be explained in terms of the ratio (V_v/r) which governs the Zener pinning effect as illustrated with steel HS140-104 that was solution treated at 1300 °C for 12 minutes, quenched into water, given a 70 percent cold deformation and isothermally annealed at 610 °C, see figure 13.2 below.

In this model, it has been assumed that all the nuclei with the estimated critical radius $r^* = 3$ nm were activated in the early stages of precipitation in what is called site saturation and that $r^* = r_o$, i.e. although the particles were very small, at time $t < P_{z(start)}$ time the volume fraction V_v was also very small $(V_v \rightarrow 0)$ and, therefore, $P_z \approx 0$. The time dependent mean particle size has been estimated by equation 4.12 $(\ln(r - r_o) = 16.4+0.85\ln(t)-14433/T)$ while the precipitation volume fraction V_v and its corresponding precipitation time has been obtained from the TTT-diagram in figure 12.15. The MAJK model for precipitation kinetics has been assumed for the transformation time between 2 and 12 minutes during the isothermal annealing process at 610 °C, and working backwards, the following expression was obtained for the volume fraction X of recrystallised material in a time t in minutes:

Chapter 13 Discussion

$$X = 1 - \exp(-0.0232t^{1.96}) \qquad (13.7)$$

The Avrami exponent of n =1.96 is in agreement with the values of between 1.4 to 2.3 which Brahmi et al[144] found in an Fe-Al-N alloy.

For Zener pinning to be effective in arresting the recrystallisation process, P_z must be above a certain critical value. In the case of the recrystallisation arrest in figure 12.12 that was observed in steel HS140-104 in the as-quenched and cold worked condition during isothermal annealing at 610 °C, the estimated critical value for P_z must be above 0.53 J mol^{-1}, see figure 13.2 below. This value may vary depending on the isothermal annealing temperature and steel composition.

As mentioned earlier, the nucleation of the AlN is over relatively quickly with effective recrystallisation arrest through Zener pinning setting in soon thereafter. The curved dashed line in figure 13.2 may, however, be a better representation of the time dependent Zener-pinning force P_z than the solid curve which was obtained from the MAJK model through equation 13.7 ($X = 1 - \exp(-0.232t^{1.96})$ which possibly underestimates the precipitation rate of the AlN. The observed early start of the recrystallisation arrest is enough evidence that there is an adequate volume fraction of AlN to induce an arrest.

Chapter 13 Discussion

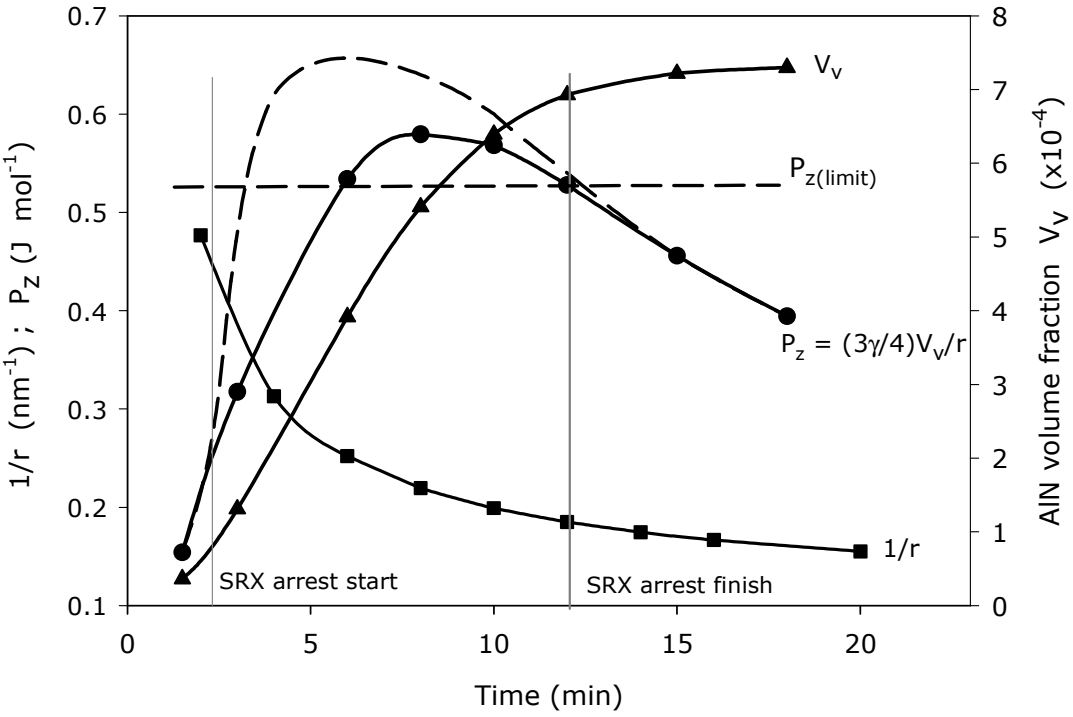

Figure 13.2: The time dependent particle volume fraction V_v, the inverse of the particle radius 1/r, and the Zener drag force $P_z = (3\gamma/4)(V_v/r)$ modelled for steel HS140-104 at 610°C after solution treatment at 1300°C, quenching into water and 70 percent cold work.

As may be seen from figure 12.12, the recrystallisation arrest times decrease with an increase in the isothermal annealing temperature. This may be attributed to the faster diffusion rates that accelerate both the recrystallisation process and the precipitation and coarsening rate of the AlN, with the latter leading to lowering of the pinning force and, therefore, to the end of arrest.

Chapter 13 Discussion

Using equation 4.12 ($\ln(r - r_o) = 16.4+0.85\ln(t)-14433/T$) that predicts the particle size as a function of time t (recrystallisation arrest time) and isothermal annealing temperature T and assuming that the end of recrystallisation arrest coincides with the end of isothermal nucleation of the AlN, and from the predicted volume fractions of AlN particles V_v (that are assumed constant) and given in table 13.3 above, the Zener drag force P_z can be modelled for steel HS140-104 in the as-quenched and cold worked condition during isothermal annealing at various temperatures. The modelled time and temperature dependent Zener-pinning force P_z at the point when it becomes ineffective is given in figure 13.3 below.

As may be seen in figure 13.3, the modelled Zener drag force P_z increased with an increase in annealing temperature and reached a peak at about 610 °C and started declining as the isothermal annealing temperature was increased further. The practical implication of this observation is that for the Zener pinning force P_z to cause recrystallisation arrest, it must lie at least above the "non-arrest" point on the curve.

The value of P_z is dependent on the particle radius $r_{(t)}$ which is dependent on temperature and time as:

$$P_z = \left(\frac{3\gamma_s}{4}\right)\left(\frac{V_v}{r_o + \exp\left[16.4 + 0.85\ln(t) - \frac{14433}{T}\right]}\right) \qquad (13.8)$$

where $r_o = r^*$ and the rest are as defined in equations 4.12 and 6.14.

The value of r in equation 4.12 ($\ln(r - r_o) = 16.4+0.85\ln(t)-14433/T$) is dependent on the isothermal annealing time (during recrystallisation arrest) t and the temperature T. Since at low isothermal annealing temperatures (<580 °C), recrystallisation can only resume when the values of P_z are low, this leads to longer recrystallisation arrest times (apparent incubation period when precipitation precedes recrystallisation) in order to allow the particles to become ineffective by coarsening. Although the Zener-pinning effect is low at lower isothermal annealing temperatures, it is still effective because of a lower diffusion and coarsening rate of the AlN particles.

The values of P_z increase with a decrease in isothermal annealing time and an increase in temperature respectively, as the AlN particle radius r is a function of both of them, until a peak is reached at about 600 °C. The decline in the values of P_z at temperatures higher than 610 °C could be attributed to the faster growth rate and coarsening rate of the AlN particles at higher isothermal annealing temperatures due to higher diffusivity of the aluminium atoms, leading to smaller values of $V_{v/}r$ again.

The observed peak in the Zener-pinning effect in figure 13.3 below has no significant practical (industrial) application as the AlN particle size in an as-coiled condition is influenced by the coiling temperature and the chemical composition of the steel.

Chapter 13 Discussion

Although the Zener-pinning force may not be substantially effective in an as-coiled condition in medium to high sulphur content steels (as it will be learnt later), the modelled results in figure 13.3 still paint a picture of its variation with isothermal annealing temperature at a time when the Zener-pinning loses its effectiveness and the recrystallisation resumes after the arrest, i.e. the point at which the AlN particles have coarsened large enough to render the Zener-pinning ineffective.

Table 13.4: Isothermal annealing temperatures and times, the modelled particle radii $r_{(t)}$ and their corresponding modelled Zener drag force P_z in J m^{-3} at the point when the recrystallisation resumes after the arrest.

Temperature (°C)	Time (min)	$r_{(t)}$ (nm)	Pz = $(3\gamma/4)(V_v/r)$ (kJ m^{-3})
640	8	14.5	35.87
625	10	13.94	38.60
610	12	8.71	43.40
580	36	21.54	30.40
550	240	77.0	11.28

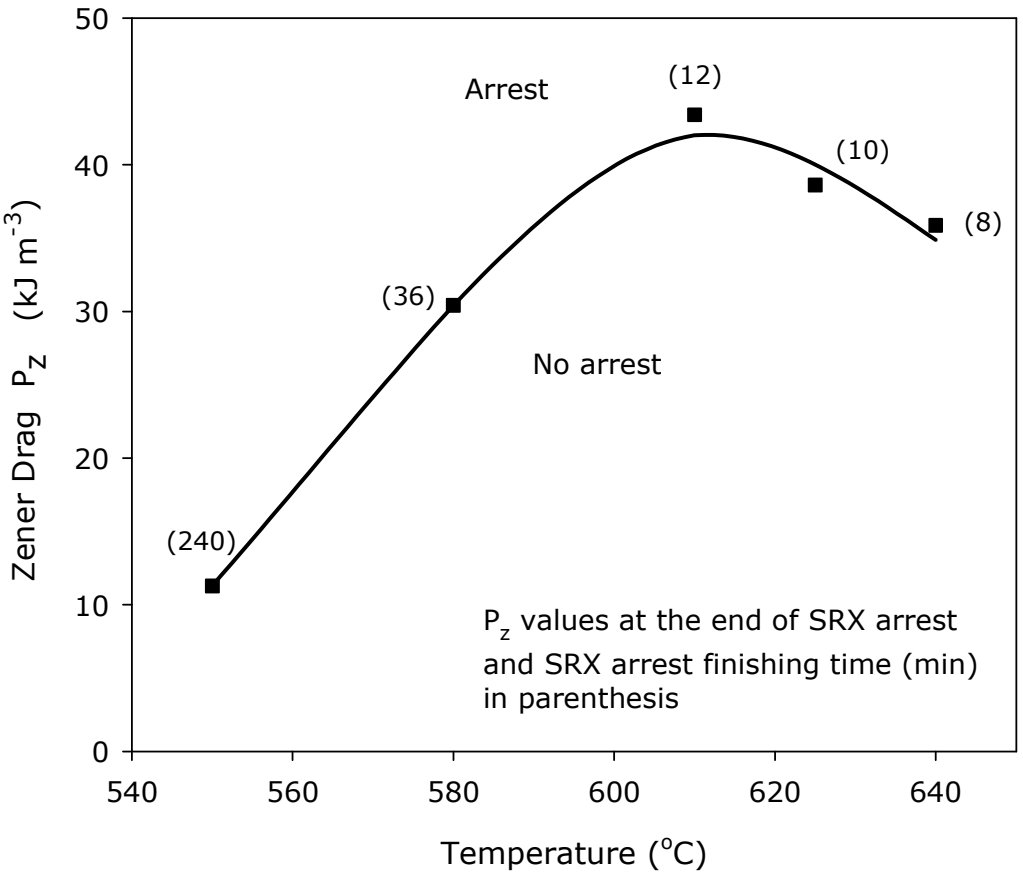

Figure 13.3: Estimated temperature and time dependent Zener drag force $P_z = (3\gamma/4)(V_v/r)$ for as-quenched steel HS140-104 at times t (in parenthesis) when the recrystallisation resumes after the arrest.

13.5 Recrystallisation behaviour in an as-coiled condition

This study was carried out on steels HS14-104, LS70-38 and LS2-65, which were hot rolled and coiled according to the schedule in table 11.1 and the heat treatment in figure 11.1. There were two parameters which were varied in this study; the coiling

temperature and the sulphur content. Two coiling temperatures were employed, i.e. 600 and 650 °C while the sulphur content varied from 2 to 140 ppm.

13.5.1 Quantitative results of the recrystallisation behaviour in an as-coiled condition

In this series of tests, steels HS140-104, LS70-38 and LS2-65 were solution treated at 1150°C for 10 minutes, hot deformed in the temperature range from 1100 to 900 °C to a total strain of 1.15, cooled at 80 °C s^{-1} to two different simulated coiling temperatures of 600 and 650 °C for 1 hour, cold worked 70 percent at room temperature and then isothermally annealed at 610 °C.

In figure 12.18, the recrystallised volume fraction at 610°C is plotted against the isothermal annealing time in the as coiled steels HS140-104, LS70-38 and LS2-65. As may be seen, in all three steels a higher coiling temperature shifted the recrystallisation process to earlier times. The higher coiling temperature did not only promote the precipitation of AlN but its coarsening as well which, in effect, reduced the Zener pinning effect on the dislocation sub-boundaries and the recrystallisation fronts.

It is also evident from figures 12.18 and 12.19 that for both coiling temperatures of 600 and 650 °C, the recrystallisation

process was shifted to longer times as the sulphur content decreased. In general, the recrystallisation start time $t_{5\%}$ increased with a decrease in the sulphur content. The sensitivity in $t_{5\%}$ to sulphur content was exacerbated by a decrease in coiling temperature to 600°C after simulated hot rolling, as the recrystallisation start time $t_{5\%}$ for the low sulphur steel LS2-65 was two orders of magnitude higher than that for the high sulphur content steel HS140-104.

As may be seen from figure 12.19, the parameter that contributed to the variations in the recrystallisation behaviour between the low and high sulphur steels was the Avrami constant k (it varied from 3.7×10^{-1} to 8.2×10^{-5} for the steels that were coiled at 600 °C) rather than the exponent n (which was $n \sim 2$ for all the three steels) as there was no large variation in the latter among these steels.

In the MAJK equation, the constant k comprises the shape factor of the nucleus, nucleation frequency and growth rate of the new grains. In both groups of steels, it was observed that nucleation of recrystallisation was by a SIBM mechanism. Since it is suggested that there is no nucleation of thermally activated embryos in this nucleation mechanism[94,99.100], the Avrami constant k in this case will strongly depend on the initial growth rate of the pre-existing recrystallisation interfaces and not on the nucleation rate per se and secondly, it will depend on how these developing "nuclei" interact with any second phase particles[89,117] that may also provide effective pinning.

Chapter 13 Discussion

This is presented schematically in figure 13.4 below in which the pre-existing recrystallisation interfaces of the low sulphur content steel are shown to take longer to grow into a critically sized "nucleus" of hemispherical shape for further growth into new recrystallised grains. The presence of the finer AlN particles in this steel reduces the net driving force for growth of these pre-existing recrystallisation interfaces through the Zener pinning effect. As was observed in the as-quenched condition above, complete recrystallisation arrest occurred in the instances where the Zener drag force P_z was greater than the net driving force for recrystallisation, equation 6.15 ($(P_{Rx} + P_c) > P_z$).

Messager et al[156] observed that the growth of dislocation sub-boundaries was more sensitive to the levels of impurities (solute atoms) through "solute drag" effects than the dislocation rearrangement during the annealing process of cold worked aluminium. In these steels studied here, instead of solute atoms, fine AlN particles are likely to have been responsible through Zener drag for the slow growth rate of the pre-existing recrystallisation interfaces in the low sulphur content steel LS2-65, thereby providing a longer effective "incubation" time. This arose in this particular steel because of a lack of MnS particles, which "forced" the nucleation of AlN to be effectively homogeneous and thus to be very fine particles.

13.5.2 Modelling the minimum value of L and the net driving force for recrystallisation P_{Rx} in steels HS140-104 and LS2-65 in an as-coiled condition

If pinning of recrystallisation interfaces by particles is the effective SIBM initiating mechanism, the recrystallisation process will be thermodynamically possible if the actual pinning distance in the steel $L_{act} > L_{min}$ where L_{min} is the minimum L value given by $L_{min} = 2\gamma_{gb}/\Delta G_{Rx}$ and ΔG_{Rx} is the driving force for recrystallisation and γ_{gb} is the surface energy of the moving interface. For the same amount of deformation energy in both steels, ΔG_{Rx} will be the same and, therefore L_{min} is given by:

$$L_{\min} = \frac{2\gamma_{gb}}{\Delta G_{Rx}} = \frac{2\gamma_{gb}}{\left(\alpha G_m b^2 N_d\right)} = 2.3\ \mu m$$

for values of $\alpha = 1$, shear modulus for iron $G_m = 8.6 \times 10^{10}$ Pa, Burger's vector for iron $b = 2.48 \times 10^{-10}$ m, estimated dislocation density for cold deformed metal $N_d = 10^{14}$ m^{-2}, ($\Delta G_{Rx} = 528$ kJ m^{-3}) and the grain boundary surface energy of $\gamma_{gb} = 1.0$ J m^{-2}.

The fact that the recrystallisation process was able to take place in both steels is enough evidence that $L_{act} > L_{min}$ and was somewhere between $L_{min} = 2.3$ μm and the observed subgrain diameter of about 5 μm (see figure 12.22). However, the kinetics of the growth of the pre-existing recrystallisation interfaces was significantly different between the two steels because in steel

Chapter 13 Discussion

HS140-104, the subgrain diameter of about 5 μm was observed after about 2 minutes while in steels LS2-65 it was found only after 240 minutes at 610°C.

The net driving force for recrystallisation P_{Rx} is given by[166]:

$$P_{Rx} = P_d - \frac{3\gamma_s V_v}{4r} - \frac{2\gamma_{gb}}{L} \qquad (13.9)$$

where P_d is given by equation 6.11, i.e. $P_d = \alpha G_m b^2 N_d$ and the rest are as previously defined in equations 6.10 and 6.14.

As may be seen from equation 13.9, recrystallisation in the SIBM mechanism will only proceed when $P_{Rx} > 0$ i.e:

$$\left|P_d\right| \geq \left|\frac{3\gamma_s V_v}{4r} + \frac{2\gamma_{gb}}{L}\right| \qquad (13.10)$$

Assuming that the values for the interface energies for the incoherent particle-matrix interface and the high angle grain boundary are $\gamma_s = 0.75$ J m^{-2} the values for P_d for the respective steels can be modelled as follows:

$$P_{d(LS2\text{-}65)} \geq \frac{3(0.75)(4.555\text{x}10^{-4})}{4(7.5\text{x}10^{-9})} + \frac{2\gamma_{gb}}{L_{act\text{-}LS2\text{-}65}}$$

$$\geq 34{,}000 + \frac{2\gamma_{gb}}{L_{act\text{-}LS2\text{-}65}}$$

Chapter 13 Discussion

and

$$P_{d(HS140\text{-}104)} \geq \frac{3(0.75)(14.665x10^{-4})}{4(57.5x10^{-9})} + \frac{2\gamma_{gb}}{L_{act\text{-}HS140\text{-}104}}$$

$$\geq 14{,}350 + \frac{2\gamma_{gb}}{L_{act\text{-}HS140\text{-}104}}$$

With finer AlN particles in steels LS2-65, $L_{act\text{-}LS2\text{-}65}$ is expected to be smaller than $L_{act\text{-}HS140\text{-}104}$, thus, assuming that the bulge is anchored by particles rather than the subgrain boundaries, i.e. $L = (4(1\text{-}V_v)r/3V_v)$ as observed by Corti et al[164]. Therefore, assuming that the grain boundary surface energy γ_{gb} is the same in both steels, steel LS2-65 will require a higher driving force P_d for recrystallisation for the condition $P_{Rx} > 0$ to be met.

The growth rate (movement) of the recrystallisation front is given by equation 6.12 ($v_B = mP_{Rx}$) and is governed not only by the mobility m of the recrystallisation front but also by the net driving force for recrystallisation P_{Rx} as well. Therefore, for the same amount of deformation energy ($\Delta G_{Rx} = P_d = \alpha G_m b^2 N_d = 528$ kJ m^{-3}) in both steels, steel HS140-104 with the higher net driving force P_{Rx}, see equation 13.9 above, is expected to have a shorter "apparent" incubation time than steel LS2-65 and this was exactly what was observed in this study. Figure 13.4 is a schematic illustration of the initial slow growth rate of the pre-existing recrystallisation interfaces of the two steels.

Chapter 13 Discussion

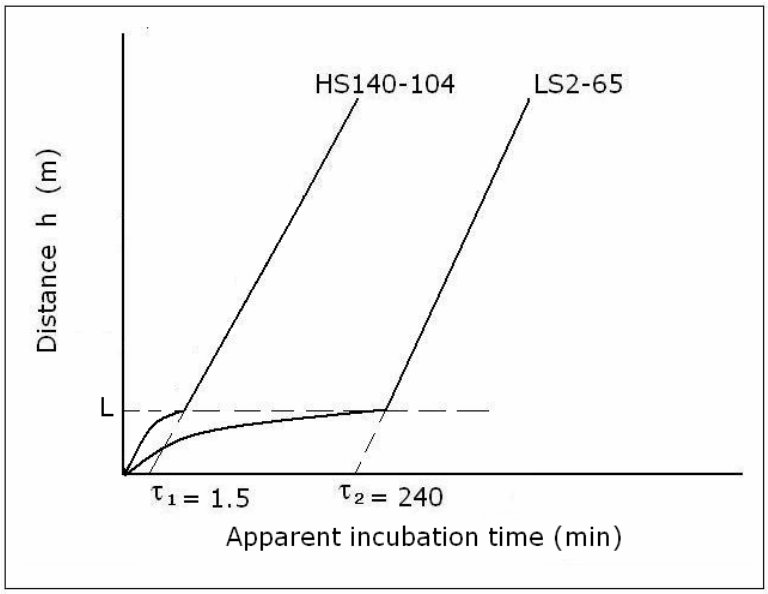

Figure 13.4: Schematic presentation of the apparent incubation time due to the initial slow movement of the recrystallisation fronts in steels HS140-104 and LS2-65 which were coiled at 600 °C and isothermally annealed at 610 °C, where $L \approx L_{min}$.

In steel HS140-104, with a dispersion factor (V_v/r) of 0.26 μm^{-1}, the recrystallisation process proceeded normally while in steel LS2-65 with a dispersion factor of 0.61 μm^{-1}, it was impeded through a longer apparent incubation period. Previous workers[165,166] on the recrystallisation of aluminium-silicon alloys observed that the early growth towards a hemisphere of the pre-existing recrystallisation interface in the SIBM mechanism, was impeded for a dispersion factor (V_v/r) > 0.2 μm^{-1}.

13.5.3 Nucleation of the recrystallised grains

In both the low and high sulphur content steels LS2-65 and HS140-104 respectively, it was observed that the nucleation of new recrystallised grains occurred on subgrain boundries and in extensively deformed areas around cementite and pearlite colonies, see figures 12.22 to 12.24. As may be seen in these figures, the new recrystallised grains continued to grow into the deformed matrix by SIBM.

The carbon content for the two steels LS2-65 and HS140-104 was 0.051 and 0.047 weight percentage respectively and, therefore, since it was not a significant variable in these steels, the cementite and pearlite colonies present in these steels and possibly acting as potential nucleation sites for recrystallisation similarly to the PSN mechanism observed in Fe-0.033%O alloy[167], may not have been different between these two steels. Hence, the availability of nucleation sites may not be one of the contributing factors to the observed difference in the recrystallisation behaviour of the steels.

As was mentioned earlier in section 6.5.2, no new recrystallisation embryos are required for the SIBM mechanism because new recrystallised grains grow from pre-existing recrystallisation interfaces and, therefore, no activation energy $\triangle G^*$ for the nucleation of thermally activated embryos and a classical incubation period τ are required. It is, therefore, the initial growth rate of these pre-existing recrystallisation interfaces to grow to a size of $L_{act} > L_{min}$ that contributes to the difference in

recrystallisation behaviour of these two groups of steels; one with high and the other with low sulphur content. It was observed that the homogeneously nucleated finer AlN particles in the low sulphur steel LS2-65 were more effective in the pinning of the dislocations, dislocation sub-boundaries and the static recrystallisation fronts, see figures 12.19 and 12.25, hence, the difference in the "apparent incubation periods" from high sulphur content steels. As may be seen in these micrographs, the AlN particles in steel LS2-65 were so small that it was only their strain fields that could be observed in the thin foils, see figure 12.25 (b).

13.6 Heterogeneous nucleation of AlN on MnS particles during hot rolling and coiling at 600 and 650 °C in low carbon Al-killed steels with various sulphur content

In this series of metallographic analysis, the steels HS140-104, LS70-38 and LS2-65 were solution treated at 1150°C for 10 minutes, hot deformed in the temperature range from 1100 to 900 °C to a total strain of 1.15, cooled at 80 °C s^{-1} to two different simulated coiling temperatures of 600 and 650 °C for 1 hour, see table 11.1 and figure 11.1. The metallographic analysis was carried out in the as-coiled condition in order to investigate the status of the AlN in all these steels prior to cold working and isothermal annealing.

13.6.1 Precipitation of AlN on MnS and its effect on static recrystallisation after cold work

In the lowest sulphur content steel LS2-65 with an absence of any MnS, the AlN nucleated homogeneously in the matrix or heterogeneously on sub- or grain boundaries during coiling, see figures 12.30 and 12.31. It was observed that these AlN particles were not only very fine (<30 nm) but sparse and infrequent and this suggested that a greater volume fraction of them were so small that they could not easily be observed in the TEM due to a lower limit of detection of about 20 nm by thin foil. The TEP results showed that after coiling for 1 hour at 600 °C, the AlN had completely precipitated as no further precipitation could be observed afterwards; see table 12.2 and figure 12.27. As opposed to the as-quenched condition, no recrystallisation arrest was observed during the isothermal annealing process in the as-coiled condition and this suggests that either partial or full precipitation of AlN had already taken place during the 1 hour coiling at 600 °C and that the particles had already grown to beyond their "full arrest size".

In the medium to high sulphur content steels HS140-104 and LS70-38, the sulphur precipitated as coarse particles of [Mn,Cu]S/MnS and [Mn,Ti,V]S/MnS respectively. Some copper sulphide particles were also observed particularly in steel HS140-104. These sulphide particles, particularly MnS, were the favoured nucleation sites for the AlN and the heterogeneous nucleation encouraged its precipitation during the coiling process after hot rolling, see figures 12.28, 12.29 and 12.33. The result was that

the AlN in medium to high sulphur content steels was generally associated with coarse sulphides and, therefore, the mean particle size of the AlN/MnS compound particles in the as-coiled steel prior to cold working and annealing, was generally much coarser, i.e. between 50 and 300 nm see figure 12.32, than in the steels with low sulphur content. Hence, no pinning of the static recrystallisation fronts was observed in these steels as may be seen from figure 12.26.

In a study[162] on the optimization of the strain aging resistance in low carbon Al-killed strip steels with 80 to 90 ppm sulphur content and which were produced by continuous annealing, it was observed that the steels with a high Mn content (0.36%Mn) were less sensitive to strain aging than those with a low Mn content (0.16%Mn) at a coiling temperature of 620 °C. This was also attributed to the heterogeneous nucleation of the AlN on MnS which promoted the precipitation of the AlN. It was concluded that the low manganese steels had provided less nucleation sites for the precipitation of the AlN hence more nitrogen was in solid solution and, therefore, caused the strain aging. These findings can be linked to the sensitivity of the low sulphur content low carbon Al-killed strip steels to the coiling temperature vis-à-vis the sluggish recrystallisation behaviour of these steels. In the absence of sulphur in the steel, there are no MnS particles which are favoured sites for the nucleation of the AlN.

Mizui et al[163] observed that there is a range of manganese content which is favourable for the optimum heterogeneous

nucleation of the AlN on these MnS particles. According to this author, an excessive increase in the manganese content of the steel can result in coarsening of the MnS particles, decreasing the density of the favoured nucleation sites for the AlN. It was also observed that the precipitation of the AlN is accelerated by an increase in the manganese level which increases the activity of the nitrogen in ferrite. Since the optimization of the manganese and the sulphur content vis-à-vis the nucleation of AlN during coiling and the recrystallisation behaviour after cold work, was not within the scope of this study, it will not be discussed further.

Although the Zener drag effect is governed by the ratio of the volume fraction of the particles V_v to the mean particle radius r (V_v/r) as stated above, in the case of the coarse MnS/AlN compound particles in the medium to high sulphur content steels it is not the V_v that matters but the particle radius r as a larger value renders the Zener drag force ineffective. Consequently, unlike in the high sulphur steels, the finer AlN particles in the low sulphur steel were more effective in retarding the recrystallisation process through the Zener pinning of the dislocation sub-boundaries and the moving static recrystallisation fronts, particularly during the early stages of the recrystallisation process before the AlN particles had coarsened and had lost their pinning effectiveness. This was summarised in figures 12.21 and 12.32 in which it is evident that the sulphur content in these steels has an indirect effect on the recrystallisation start time $t_{5\%}$ though its influence on the particle size of the AlN. The empirical equations that relate the sulphur content in ppm to the static

recrystallisation start time $t_{5\%}$ in minutes in these steels are given in table 12.2 and are as follows:

$$t_{5\%} = 33.78\exp(-0.0345S) \text{ for } 600\ ^\circ C \qquad (13.11)$$

and

$$t_{5\%} = 0.99\exp(-0.008S) \text{ for } 650\ ^\circ C. \qquad (13.12)$$

13.6.2 Modelling of the $\triangle G_v$, $\triangle G^*$ and r^* for the nucleation of AlN, Cu_2S and MnS in austenite and ferrite

In order to understand the sequence of precipitation of the MnS, AlN and Cu_2S in these steels, it is necessary to know both the thermodynamics and the kinetics of the formation of these species. The kinetics are presented in the TTT-diagrams which are in figures 4.1, 4.2 and 5.1. The parameters that have been used to model the driving force $\triangle Gv$, activation energy $\triangle G^*$ and the critical radius r^* for the homogeneous nucleation of AlN, Cu_2S and MnS in austenite and ferrite, are given in table 13.5 below. The enthalpies of formation have been derived from the equilibrium solubility equation using equation 4.3 ($\triangle H = 1.15RA$). The activation energy $\triangle G^*$, the critical radius r^* and the driving force $\triangle Gv$ have been calculated from equations 3.5, 3.6 and 3.7 respectively and these parameters have been plotted as a function of temperature in figure 13.5 below.

Table 13.5: Parameter values for the calculations of ΔGv, ΔG* and r* for the homogeneous nucleation of MnS, AlN and Cu_2S in austenite and ferrite.

Compound	Solubility model	Parameter	Value	Ref.
MnS	$Log[\%Mn][\%S]=10.6-\frac{19427}{T}$ $Log[\%Mn][\%S]=4.092-\frac{10590}{T}$	ΔH_{aust} (J mol^{-1}) ΔH_{ferr}	82500 101300	66 157
		γ_{aust} (J m^{-2}) γ_{ferr}	0.712 1.024	158
		V_m (m^3 mol^{-1})	2.164 x10^{-5}	
		a (fcc) (nm)	0.522	
AlN	$Log[\%Al][\%N]=2.44-\frac{9490}{T}$ $Log[\%Al][\%N]=6.1-\frac{14442}{T}$	ΔH_{aust} (J mol^{-1}) ΔH_{ferr}	90800 138000	Present work 49
		γ_{aust} (J m^{-2}) γ_{ferr}	0.75 0.2	151
		V_m (m^3 mol^{-1})	1.28 x10^{-5}	
		a (fcc) (nm)	0.311	36
Cu_2S	$Log[\%Cu]^2[\%S]=26.3-\frac{44971}{T}$	ΔH_{aust} (J mol^{-1}) ΔH_{ferr}	286900 286900	159
		γ_{aust} (J m^{-2}) γ_{ferr}	0.83 0.2	160
		V_m (m^3 mol^{-1})	2.751 x10^{-5}	
		a (fcc) (nm)	0.522	62

Chapter 13 Discussion

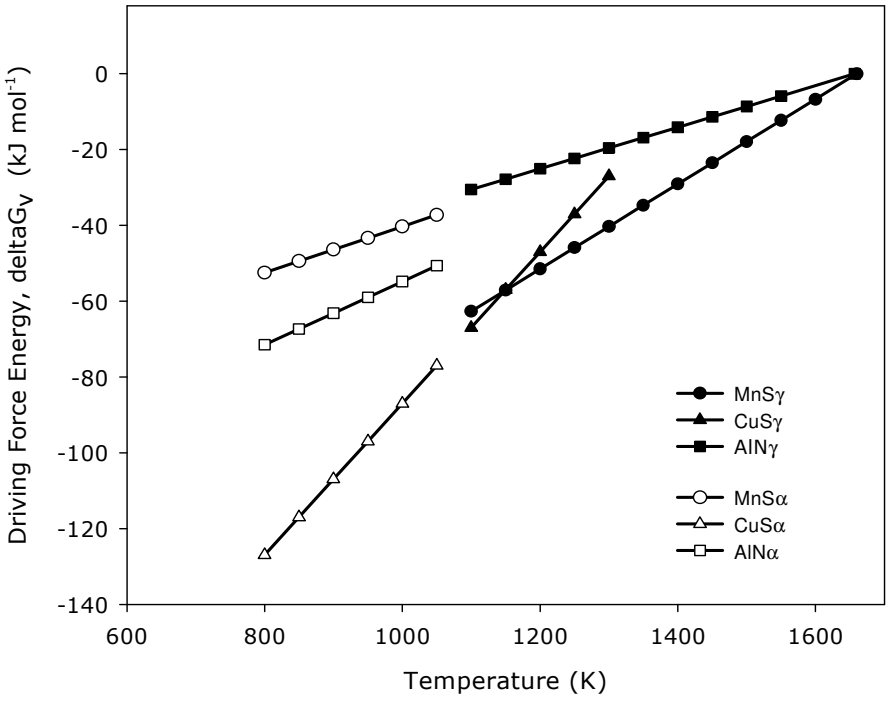

(a)

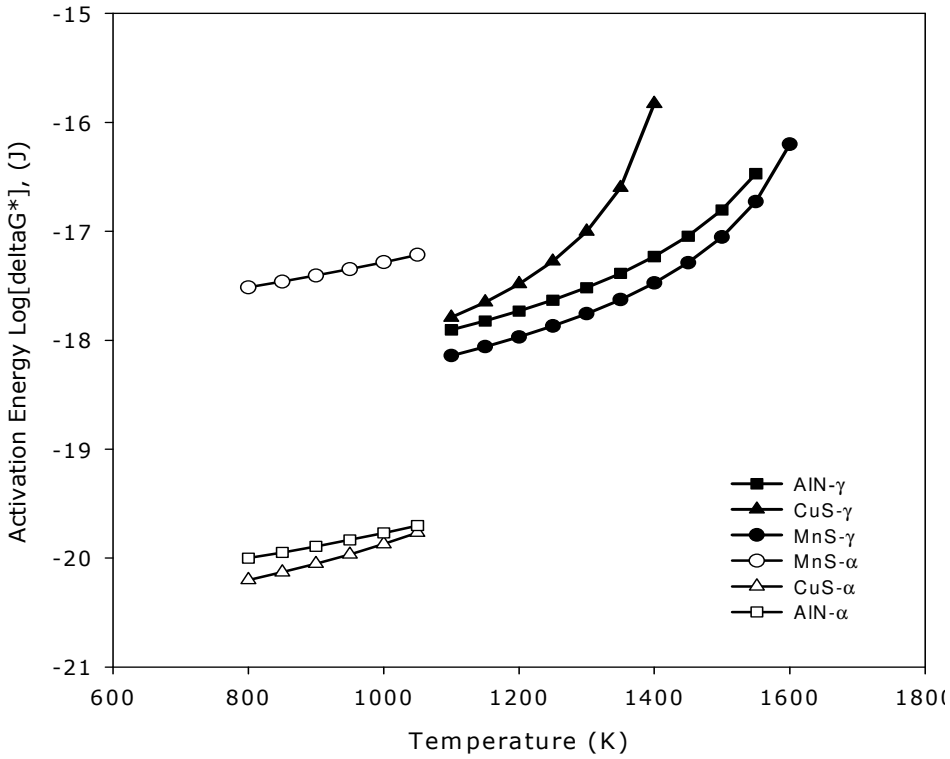

(b)

Chapter 13 Discussion

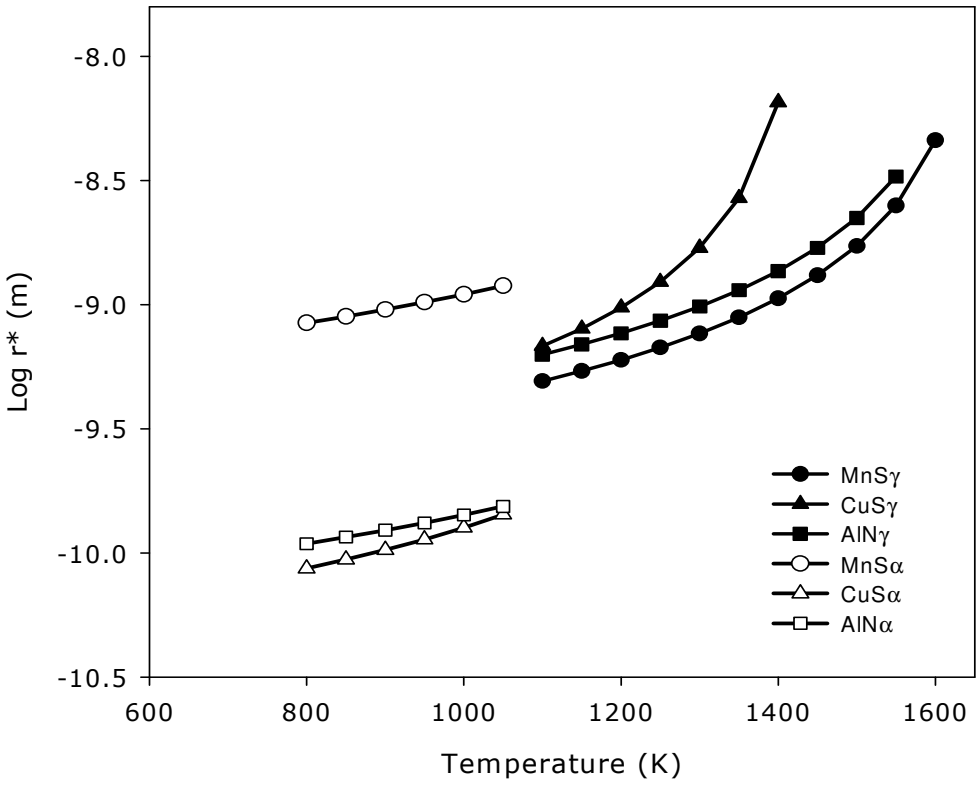

(c)

Figure 13.5: (a) Modelled driving force ΔG_v, (b) activation energy ΔG^* and (c) the critical radius r^* for the homogeneous nucleation of AlN, Cu_2S and MnS in austenite and ferrite. Solid symbols are for austenite and open ones for ferrite.

The general conclusion from figure 13.5 may be that, on the one hand, it is easier for the AlN to precipitate in α-ferrite than in austenite as both the activation energy ΔG^* and the critical radius r^* are less by two orders of magnitude while the driving force ΔG_v is higher by 20 kJ mol^{-1} compared with the values for MnS. On the other hand, it is easier for the MnS to precipitate in austenite as the activation energy ΔG^*, and the critical radius r^* are less while the driving force ΔG_v, is higher than those of the

AlN. This confirms the previous observations from other workers that AlN forms readily in ferrite without any incubation period being observed due to the higher diffusivity of aluminium and low lattice misfit δ attained through the Bain orientation between the α-ferrite matrix and the cubic (NaCl type) crystal structure AlN[11,44,66]. As others have suggested, the nucleation of AlN within austenite is limited by the nucleation barrier of hcp AlN in austenite[44].

Thermodynamically, it is known that MnS forms at higher temperatures than AlN and is normally present first upon cooling, see the ThermoCalc results in figure 12.4. As may be seen in figure 13.5 (b) and (c), AlN may precipitate easier in austenite than Cu_2S does as both ΔG^* and r^* are less for the latter. Therefore, it is logical to conclude that the AlN generally rather precipitates heterogeneously on MnS as found here and by others[52,60,162,163]. The crystallographic orientation relationship between the AlN and the MnS was found to be $(1\bar{1}1)_{MnS}//(0001)_{AlN}$ and $[110]_{MnS}//[2\bar{1}\bar{1}0]_{AlN}$ (see figure 12.33) as observed by others[52].

14. 1 Conclusions

The following conclusions were drawn from this study:

14.1.1 Low carbon Al-killed strip steels in the as-quenched condition

- The TEP technique was successfully used to study the equilibrium solubility of AlN during reheating of low carbon Al-killed strip steels ranging from low to high sulphur content and it was found that the sulphur content does not influence the equilibrium solubility of the former, thus, regardless of the association of the AlN with the MnS in the medium to high sulphur content steels. The equilibrium solubility equation thus obtained was determined as:

$$\mathrm{Log}[\%\mathrm{Al}][\%\mathrm{N}] = 2.6 - \frac{9710}{\mathrm{T}}$$

where the aluminium and the nitrogen contents are in weight percentages and T is the absolute solution temperature in Kelvin.

- During solution treatment at 1150 °C, the equilibrium dissolution of AlN in these steels was, in general, attained after soaking for 5 minutes or more. It may, therefore, be concluded that AlN dissolves relatively quickly in low carbon Al-killed strip steels during a solution or reheating treatment, regardless of the process route, i.e. whether it is the cold charge or hot charge route.

- In the as-quenched condition of both the low and high sulphur content Al-killed steels, a recrystallisation arrest was found at some isothermal annealing temperatures. The recrystallisation arrest was associated with the diffusion of aluminum atoms with an activation energy of the process that led to the arrest, being 230 kJ mol^{-1}. This is reasonably close to the published activation energy for the diffusion of aluminium in ferrite. The arrest appeared to be caused by Zener pinning by the precipitating AlN and was not affected by the sulphur content of the steel in solid solution. Recrystallisation arrest occurred in these steels with an estimated volume fraction of AlN particles of 4.6 $x10^{-4}$ or more and not in steels with a volume fraction of 2.7 $x10^{-4}$ or less.

- The total time over which arrest occurred, was a function of the annealing temperature and the termination of arrest and resumption of recrystallisation appeared to be governed by the end of precipitation of any new AlN and/or its coarsening to a point where the Zener pinning force $P_z = f(V_v/r)$ became ineffective. For steel HS140-104, in the as-quenched condition and during isothermal annealing at 610 °C, this was found to be $P_z \leq 0.53$ J mol^{-1} (41.2 kJ m^{-3}).

- The recrystallisation arrest was only observed in the medium to high nitrogen content steels with the volume

fraction $V_v \geq 4.56 \times 10^{-4}$ or a nitrogen content of about 65 ppm and higher.

- Since the start and termination of recrystallisation arrest appeared to be linked to the precipitation of the AlN, it was possible to derive an estimated TTT-diagram from the arrest data in those steels where this effect was found.

- In the as-quenched condition and through Johnson-Mehl-Avrami-Kolmogorov plots, it was established that the incubation time of the recrystallisation process increased with an increase in sulphur content in solid solution of the steels. However the kinetics of the recrystallisation process were not influenced by the sulphur content with a JMAK exponent of $n \approx 1$ for all the steels tested and neither was the sulphur content associated with the arrest phenomenon. Consequently, the recrystallisation process was shifted to longer times with an increase in sulphur content in solid solution, possibly through sulphur drag as has been suggested by others.

14.1.2 Low carbon Al-killed strip steels in the hot deformed and as-coiled condition

- In a hot deformed and as-coiled condition where the sulphur had precipitated fully as MnS before the recrystallisation started, the JMAK incubation period of the recrystallisation process decreased with an increase in the sulphur content of the steel. This was found to be due to the MnS particles that are the favoured nucleation sites for the AlN and the

heterogeneous nucleation enhanced the precipitation of the latter. The resulting compound and coarse AlN/MnS particles were generally ineffective in pinning any dislocation sub-boundaries and recrystallisation fronts and consequently had little or no effect on the recrystallisation process.

- In the very low sulphur content steels, however, the absence of any significant quantities of MnS forced the AlN to nucleate as much finer particles on dislocations and subgrain boundaries where effective Zener pinning was once again observed, leading to a much delayed start of recrystallisation but not to any actual recrystallisation arrest.

- The sensitivity of the recrystallisation start time (JMAK incubation time) to the sulphur content increased with a decrease in the coiling temperature as the finer homogeneously nucleated AlN particles remained smaller at the lower coiling temperatures (~ 600°) due to a slower coarsening rate. The sulphur (ppm) dependent empirical expressions for the recrystallisation start times $t_{5\%}$ at isothermal annealing temperature of 610 °C for steels coiled at temperatures of 600 and 650 °C were found to be:

$t_{5\%} = 33.78\exp(-0.0345S)$ for 600 °C and

$t_{5\%} = 0.99\exp(-0.008S)$ for 650 °C.

- The kinetics of the recrystallisation process were not influenced by the sulphur content with a JMAK exponent of $n \approx 2$ for all the steels tested. However, it was the JMAK constant k that differed much with the sulphur content and the coiling temperature, decreasing with the decrease in either one or both of them.

- The sulphur content in these hot worked and coiled low carbon Al-killed strip steels, therefore, plays an indirect role in the recrystallisation process after cold work by affecting the mode of nucleation of the AlN, thereby, making it either effective or ineffective in its Zener pinning force on moving recrystallisation fronts. This finding is, therefore, the main reason for the large differences found within industry in the recrystallisation behaviour of nominally equivalent steels but with varying sulphur contents, an observation that originally led to this study.

14.2 Recommendations

The following recommendations were also drawn from this study:

- Tentatively, a medium to high sulphur content of 50 to 100 ppm would be appropriate to solve the "sluggish" recrystallisation problem in these steels. However, a comprehensive study to optimize the sulphur content vis-à-vis the kinetics of the recrystallisation process and the

mechanical properties, particularly deep drawability, would be valuable.

- A higher coiling temperature (~ 650 °C) would help to alleviate the problem; however, there is a limit in taking this route because there are usually temperature gradients in the coil, with the outer wraps and the edges being cooler than the center. Higher coiling temperatures may also result in difficulties in the removal of scale from the coiled strips. Hence, increasing the sulphur content seems to be a better option.

- Since the sulphur content both directly and indirectly affects the recrystallisation behaviour of these low carbon Al-killed strip steels, there is a likelihood that the recrystallisation texture of these steels may be affected as well. Therefore, a study of the influence of the sulphur content on the development of the recrystallisation texture in these steels would be appropriate.

- In the medium to high sulphur content steels, the AlN is not only associated with MnS but with [Mn,Cu]S and [Mn,Ti,V]S complexes and it appears that there is an information gap in the literature in the understanding of the crystallographic orientation relationship of the AlN with these particles and whether their heterogeneous nucleation enhancement of the AlN may differ from that of MnS itself.

- In low sulphur content steels where the finer AlN plays a direct role in delaying the recrystallisation process, a study of the kinetics of coarsening of AlN would also be helpful as it may be used to optimise the coiling temperature vis-a-vis the subsequent cold worked recrystallisation behaviour.